

# Leaky Frontends: Security Vulnerabilities in Processor Frontends

Shuwen Deng, Bowen Huang, and Jakub Szefer  
Yale University  
{shuwen.deng, bowen.huang, jakub.szefer}@yale.edu

**Abstract**—This paper evaluates new security threats due to the processor frontend in modern Intel processors. The security threats are based on new timing and power covert channels. The root causes of the security threats are the multiple paths in the processor frontend that the micro-ops can take: through the Micro-Instruction Translation Engine (MITE), through the Decode Stream Buffer (DSB), also called the Micro-op Cache, or through the Loop Stream Detector (LSD). Each path has its own unique timing and power signatures, which lead to the security threats presented in this work. In addition, the switching between the different paths can lead to observable timing or power differences which could be exploited by attackers. Because of the different paths, the switching, and the way the components are shared in the frontend between hardware threads, two separate threads are able to be mutually influenced and timing or power can reveal activity on the other thread. The security threats are not limited to multi-threading, and this work further demonstrates new ways for leaking execution information about SGX enclaves or a new in-domain Spectre variant. In addition, this work demonstrates a new method for fingerprinting the microcode patches of the processor by analyzing the behavior of different paths in the frontend. This work demonstrates that the whole processor frontend needs to be considered when ensuring the security of processor architectures.

## I. INTRODUCTION

The processor frontend is responsible for fetching, decoding and delivering instructions to the rest of the processor pipeline. To enhance performance and reduce power, multiple paths for instruction decoding and delivery are widely adopted in today’s processor designs, such as from Intel [1]. The design of the frontend also ensures that ideally it will not become a bottleneck, so that the backend is always fed with sufficient instructions to process. Consequently, majority of timing or power variations that can be observed in processors are due to components in the backend as that is the bottleneck where execution differences can be more easily observed. This has resulted in numerous security vulnerabilities that have been previously uncovered, e.g., [4], [13], [15], [19], [36].

Meanwhile, we study security of the multiple paths in the processor frontend that the micro-ops can take: through the Micro-Instruction Translation Engine (MITE), through the Decode Stream Buffer (DSB), also called the Micro-op Cache, or through the Loop Stream Detector (LSD). In addition, we study the switching between these different paths and how it could be exploited by attackers. The security study of the processor frontend is largely unexplored. The frontend paths include MITE, DSB, and LSD. The DSB and LSD were first introduced starting from Intel Core microarchitectures to

improve performance and power and to augment the previously existing MITE. As the result, in today’s processors, the same instruction can possibly go through 1 out of 3 different paths: MITE, DSB, or LSD. The instruction decoding in the processor frontend then has a unique feature where the same instruction decoding and delivery of micro-ops can take different paths. This has important implications: each instruction (or its decoded micro-ops) can be concurrently located in up to three structures: MITE, DSB, and LSD. The execution timing and power depend on the exact path taken in the frontend. In addition, different events can cause switching of the paths based on the activity in the different threads, loop sizes, or instruction prefixes used, and the switching can also lead to timing and power differences. The different paths are basis of the vulnerabilities that we demonstrate in this work.

The frontend vulnerabilities are different and independent from speculative attacks [5], [7], [16], [18], [27], [29], branch predictor attacks [10], [11], or processor backend attacks [4], [15], [19], [36]. All these attacks happen after the instructions have already been decoded. Nevertheless, the frontend vulnerabilities can be used, e.g., as new channels in a Spectre attack, as we demonstrate.

Our multi-threaded (MT) attacks use different threads for the sender and the receiver, and leverage evictions or misalignments in DSB or LSD to create different timing or power variations that can be measured by the receiver. For all the attacks, the attacks only affect the frontend and do not, for example, cause interference in the L1 instruction (L1I) caches. The multi-threaded attacks can further be applied to attack SGX enclaves. We also present attacks that do not require multi-threading (non-MT) and mainly use internal-interference among the sender’s own code to cause timing or power variations that the attacker can measure. The non-MT attacks can be applied to both SGX or as a new in-domain Spectre attack. In addition to new attacks on the frontend itself, we demonstrate fingerprinting approach that can use frontend behavior to determine which processor microcode patches have been applied. Knowing which microcode patches have been applied can let attacker stage further attacks by knowing which patch has or has not been applied.

For the different attacks and fingerprinting, timing can be measured by unprivileged attackers. The power meanwhile can be measured by attackers that can access energy counters, e.g., Intel’s Running Average Power Limit (RAPL) [1], available in today’s processors. The attacks can thus be done in software and remotely, and part of our evaluation uses public,

cloud-based servers for attack demonstration.

### A. Contributions

The contributions of this paper are:

- Design of covert channels making use of eviction and misalignment of DSB and LSD entries.
- Development of frontend attacks which can covertly send bits between hyper-threads or on the same thread in time-sliced setting using internal-interference.
- Design of both timing-based and power-based variants of the attacks.
- Development of attacks leveraging special instruction prefixes to force frontend path switches.
- Demonstration of the frontend attacks’ ability to leak information from Intel SGX enclaves.
- Demonstration of the use of the frontend covert-channels as part of a new Spectre attack variant.
- Development of frontend fingerprinting to detect which microcode patch has been applied.

### B. Responsible Disclosure and Open-Source Code

Our research findings have been shared with Intel. We are in discussion with Intel about open-sourcing our attack code when it is safe to do so.

## II. BACKGROUND

Various microarchitectural optimizations have emerged in past years as sources of security vulnerabilities. Researchers have focused mainly on attacks leveraging features in the processor backend, while this work focuses on processor frontend timing-based and power-based attacks to bring awareness that processor frontend needs to be considered when ensuring security of processor architectures.

Previously, security vulnerabilities have been uncovered which are caused by all the different levels of caches [4], [15], [19], [36], port contention in the execution engine [3], branch predictors [10], [11], or memory controllers [33], for example. Security community has especially focused on the speculative execution attacks, following Spectre [5], [7], [16], [27], Meltdown [7], [18], Foreshadow [30], [34], and various more recent attacks [2], [6], [26], [31], [31], [32]. Other recently explored vulnerabilities include attacks that abuse branch prediction, but not for Spectre-like attacks. This includes BranchScope vulnerability [11] or Jump over ASLR type vulnerabilities [10]. There are also attacks that leverage prefetchers [14] and value predictors [9]. Most recently, researchers have also demonstrated microarchitectural replay attacks [28] and attacks abusing network-on-chip (NoC) [23].

The vulnerabilities that we present meanwhile focus on the frontend. To the best of our knowledge, there is only one independent work that has explored frontend and the micro-op cache (also called DSB) for security attacks [24]. The work focused on studying eviction of DSB and how it can cause timing differences that attackers can exploit. Compared to the work [24], we are able to 1) present both eviction-based and misalignment-based attacks that leverage the DSB,

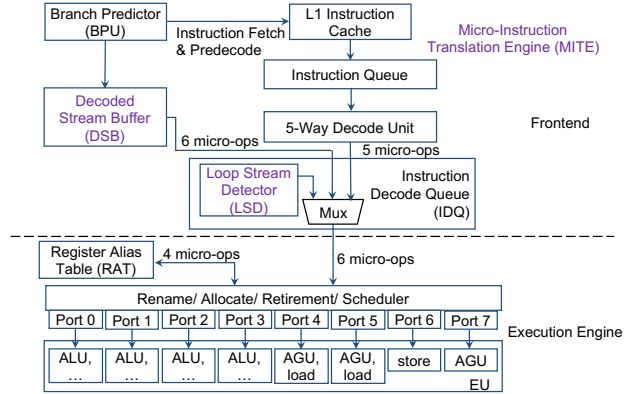


Fig. 1: Microarchitecture details of the frontend and the execution engine, based on [1].

LSD, and MITE, 2) show new power attacks, 3) evaluate SGX attacks, 4) analyze LSD influence, 5) use frontend behavior for microcode patch fingerprinting, and 6) analyze instruction prefixes causing switching in the frontend paths for new attacks. We believe our work complements existing work by providing new attacks and security insights, including, to the best of our knowledge, fastest frontend attack reaching 1.4Mops.

### A. Threat Model and Assumptions

This paper focuses on analyzing security of remote attacks, such as when the victim and the attacker are co-located on the same server, but attacker does not have physical access to the machine. We assume there is one sender (victim) that holds security-critical information and one receiver (attacker) that tries to extract the secret information by measuring timing and power changes. We demonstrate vulnerabilities in both hyper-threading setting (Section IV-A and IV-B) where the two run in different hardware threads sharing the same core, and attacks in single-threaded setting (Section IV-C, IV-D, and IV-E) where the victim and the attacker are time-sharing the code. Attacks on SGX (Section VII) assume the attacker can trigger execution of the enclave and measure its timing or power. New Spectre attack (Section VIII) assumes an in-domain attack scenario: the attacker is within same thread, e.g., as a sandboxed code where the disclosure gadget is executed. The fingerprinting attack (Section IX) assumes attacker has prior access to the same CPU as the target one, so they can measure frontend performance under different microcode patches. All of the timing-based attacks can be performed fully from the user-level privilege using the `rdtscp` instruction for measuring timing, but alternate timing methods such as a counting thread can be used if precise timing instruction is not available. The power channels require access to Intel’s RAPL [1] to get energy information. Even if the RAPL access is disabled for user-level code, privileged code can still use the power channels against SGX enclaves, for example.

## III. ANALYSIS OF FRONTEND OPERATION

Within the processor frontend, instruction decoding and delivery to the backend has multiple paths through the Micro-

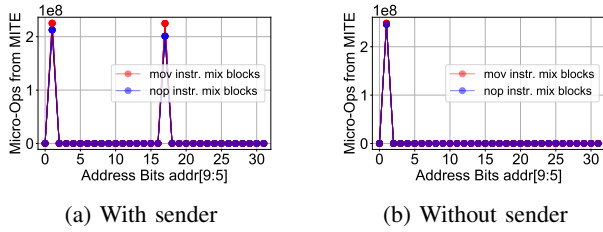


Fig. 2: Increased MITE micro-op numbers show that when two threads are running, the DSB is partitioned. Although there are 32 physical sets, with two threads running, each thread gets 16 sets. Within a thread, addresses that map to sets offset by 16, e.g., set 1 and 17, conflict with each other in DSB and cause internal-interference.

Instruction Translation Engine (MITE), the Decoded Stream Buffer (DSB), also called the micro-op cache, and the Loop Stream Detector (LSD), as is seen from Figure 1.

Given that MITE path has low throughput and high power consumption, the DSB has been added and the micro-ops decoded by MITE are inserted into the DSB [1] in modern Intel processors. If the micro-ops are available in the DSB, the micro-op stream is sent directly from DSB to the IDQ, bypassing the MITE, therefore saving power and improving throughput. The instruction delivery path from DSB is also shorter than MITE (shorter by 2 – 4 cycles), so the pipeline latency is reduced as well [1].

Further, there is also the LSD located within the IDQ. If the micro-op stream belongs to a qualified loop (discussed in Section III-A4), then all the micro-ops belonging to the loop code can be issued directly from LSD to the backend, bypassing DSB as well. The purpose of the LSD is to help save power, but it also can help performance by providing higher instruction delivery throughput. When branch mis-prediction occurs, for example at the end of the loop, or the number of micro-ops within the loop exceeds the limit that the LSD can handle, LSD is not used and micro-ops are delivered from the DSB. Furthermore, if the micro-ops exceed the DSB limit or belong to a newly accessed micro-ops, they are processed by the MITE. Further, DSB is inclusive of LSD and MITE is inclusive of DSB as well [1], e.g., eviction of micro-ops from DSB will cause their eviction from LSD as well.

### A. Controlling Use of the Frontend Paths

In this section we discuss what code sequences can be used to achieve execution through the different frontend paths.

1) *Controlling How LSD is Used:* The LSD can continuously stream the same sequence of up to 64 micro-ops, directly from the IDQ to the backend [1]. While the LSD is active, the rest of the frontend is effectively disabled. In order to generate detectable timing and power difference between LSD vs. DSB and DSB vs. MITE, one can control the number of micro-ops within a loop to either make it fit in the LSD, so that instruction delivery starts with LSD only, or exceed the LSD limit so the processor falls back to using DSB or MITE, creating timing and power differences that can be detected.

2) *Controlling How DSB is Used:* The DSB is constructed as a cache-like structure with 32 sets and 8 ways per set [1]. Each line can store up to 6 micro-ops or 32 bytes (so DSB

can hold at most 1536 micro-ops in total). Based on our reverse engineering as well as Intel manuals [1], we find that when there is only one thread running on the hardware core, instructions’ virtual address bits  $addr[4:0]$  are used as the byte offset within the 32-byte window, and  $addr[9:5]$  are the set index bits into the 32 DSB sets. However, when two threads are running in parallel on the hardware core, the DSB is set partitioned, and half the sets are assigned to each thread from the experimental results.

Although the DSB is partitioned when two threads are running, we observe that when only one thread is active, the thread is assigned to all the DSB sets. To test this, we created two threads accessing a set of *mov* or *nop* instructions within a loop containing 20 million iterations and we let them run in parallel in the same hardware core. The first thread always accesses 8 32-byte blocks of instructions which all have same  $addr[9:5]$  bits. In parallel, second thread access 8 32-byte blocks of instructions where  $addr[9:5]$  bits are set to all the possible values from  $00000_2$  to  $11111_2$ . As is shown in Figure 2a, second thread experiences increased MITE usage (and thus DSB evictions) for  $addr[9:5]$  bits which are exactly 16 apart, confirming that with two threads, the DSB is partitioned. Meanwhile, when only one thread is running (shown in Figure 2b), there is no increased MITE usage for  $addr[9:5]$  bits which are exactly 16 apart, indicating that a single thread gets all 32 sets when running by itself.

Figure 2 was tested on Intel Xeon E-2174G with LSD disabled to show the collisions are not influenced by LSD. We also tested on Intel Gold 6226 with LSD enabled, and observe similar results. Further, we tested Intel Gold 6226 with LSD enabled, but each thread was set to access larger blocks of instructions which do not fit in LSD (forcing processor to use DSB even if LSD is enabled), and similar results are observed.

3) *Validating Source of Observed Frontend Timing Differences:* To validate the timing changes observed are indeed due to different execution paths used, we performed a set of experiments which access  $\{40, 400, 4000\}$  *mov* instructions in a loop that is repeated 20 million times, to keep the same number of loops for each experiment. Consequently, the experiments execute in total  $\{800 \text{ million}, 8,000 \text{ million}, 80,000 \text{ million}\}$  *mov* instructions, respectively. The loop with 40 micro-ops will directly use LSD (if it is enabled in the processor) since 40 micro-ops is within the 64 micro-op limit of the LSD capacity. The loop with 400 micro-ops will not be able to use LSD due to the loop size and force the micro-ops processed in the DSB. Since the capacity of DSB (1536 micro-ops) can hold 400 micro-ops from the loop, the MITE is not used. The loop with 4000 micro-ops will force the use of both DSB and MITE since the DSB can hold some (up to 1536) micro-ops but not all, and extra micro-ops go through MITE. We did not find a way to force the use of MITE only, thus the three possible paths are using LSD (for small loops), DSB (for medium loops), and MITE+DSB (for large loops).

To verify the timing changes are indeed due to different frontend paths used for micro-op delivery, we use Linux *perf* tools [8] to measure 800 million number of micro-ops delivered by MITE, DSB, and LSD for loops with different number of micro-ops. The representative results from two

TABLE I: Specifications of the tested Intel CPU models.

Model	Gold 6226	Xeon E-2174G	Xeon E-2286G	Xeon E-2288G
Microarchitecture	Cascade Lake	Coffee Lake		
Core Number	12	4	6	8
Thread Number	24	8	12	8 <sup>a</sup>
L1D Configuration	32KB, 8-way, 64 byte line size, 64 sets			
DSB Configuration	8-way, 32 byte window, 32 sets			
LSD Entries	64	— <sup>b</sup>	— <sup>b</sup>	64
Frequency	2.7GHz	3.8GHz	4.0GHz	3.7GHz
OS	18.04 Ubuntu			
SGX Support	No	Yes		

<sup>a</sup> We use Xeon E-2288G on Microsoft Azure cloud, this processor model is specific for Microsoft Azure and has hyper-threading disabled, although hyper-threading is supported by other E-2288G processors. <sup>b</sup> LSD is disabled in these machines.

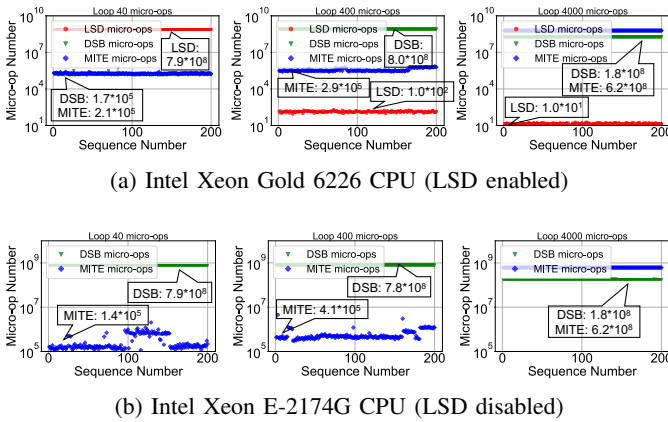


Fig. 3: Performance counters for the different experiments. With small loops LSD (if present) indeed services the most micro-ops. For medium loops DSB handles most micro-ops, and for largest loops both MITE and DSB handle most micro-ops. This confirms that the experiments correctly trigger the different paths – and that resulting timing is related to the paths used. The numbers in the call-out boxes are the average micro-ops numbers for all the 200 rounds of experiments.

machines are shown in Figure 3.<sup>1</sup> It can be clearly seen that for Intel Gold 6226 processor, when looping with 40 and 400 micro-ops, most of the micro-ops are processed by LSD and DSB, respectively. When looping with 4000 micro-ops, most of micro-ops are processed by both MITE and LSD. LSDs of E-2174U and E-2286U are disabled but the DSB and MITE processing differences are still clearly observable between loops with 400 and 4000 micro-ops. Micro-op delivery of MITE also differs between loops with 40 and 400 micro-ops. Real attackers would not have access to these counters. We showed these only to validate our findings.

4) *Ensuring Observability of Frontend Timing:* When the DSB is used for instruction delivery, it can process at most 32 bytes or 6 micro-ops per cycle. However, the Register Alias Table (RAT) and retirement unit in the backend can

<sup>1</sup>Performance counters are disabled for Intel Xeon E-2288G processor in Microsoft Azure, so counter data is not shown. Intel Xeon E-2286G CPU performance number results are similar to Intel Xeon E-2174G CPU, so only data for E-2174G is shown.

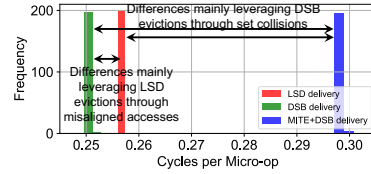


Fig. 4: Example time histogram of Intel Xeon Gold 6226 processor of using LSD, DSB, or MITE+DSB paths. Timing difference between LSD/DSB and MITE+DSB are used for collision-based attacks (see Section IV-A) and differences between LSD and DSB paths are used for misalignment-based attacks (see Section IV-B).

only process 4 micro-ops per cycle at most. Therefore the maximum instructions per cycle (IPC) is hard-limited to be 4 by the rename and retire unit not counting instruction fusion.

Because the issue-widths of the frontend and the backend are not identical, in order to be able to observe any timing or power changes due to the frontend, one needs to carefully set up the instruction mix used to make sure the instruction delivery of frontend is the bottleneck.

For example, Intel Skylake has 8 execution ports in the backend to process micro-ops, but each port can only process certain types of micro-ops. Also, a DSB line will be ended by a branch instruction or a complex instruction even if the instruction stream does not entirely fill the DSB line. Such limitations create restrictions on the instruction mix that can be used to create bottlenecks in the frontend.

To achieve high backend throughput so that the frontend is the bottleneck, we do not want to touch data-related operations such as load and store because memory system may cause unpredictable timing differences, which are not due to frontend path changes. Load and store operations would also likely leave traces in the caches which may make any attacks more detectable. Based on our analysis and above limitations, instruction mix sequence which maximizes the timing signature of the frontend for our attacks should satisfy the following three requirements:

- Total bytes of one access block should not exceed 32 byte window (e.g., 4 *mov* and 1 *jmp* use in total 25 bytes).
- Total micro-op number should not exceed 6 micro-op limit that DSB can process by one DSB line (e.g., 4 *mov* and 1 *jmp* are decoded to total 5 micro-ops).
- Avoid port contention. The 4 *mov* instructions exploit the ports as much as possible, plus 1 *jmp* instruction to end the cache line block, while avoiding load, store, or more complex instructions involved, which will cause influence or noise from other microarchitectural units.

As the result, 4 *mov* plus 1 *jmp* sequence is the *instruction mix block* which fits the requirement. Other instruction mix blocks are possible, although finding sufficient type and number of instruction mix blocks in real code may be a limitation of the proposed attacks.

5) *Exploiting Frontend Path Timing Differences:* As can be seen from histogram of Intel Xeon Gold 6226 processor shown in Figure 4, the timing difference of processing instruction mix blocks using DSB vs. MITE+DSB or LSD vs. DSB are clearly visible. In our attacks discussed later, we will use DSB

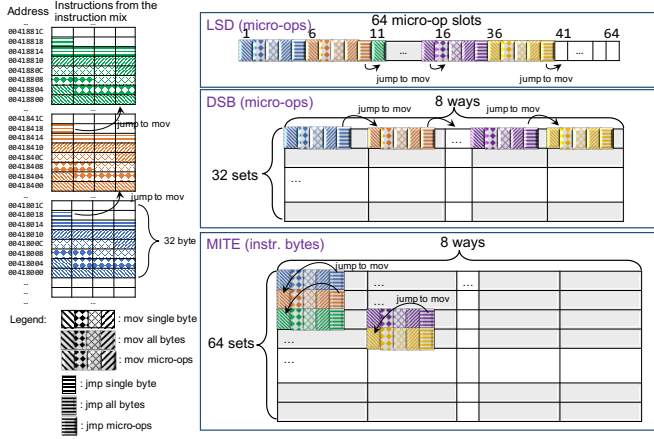


Fig. 5: Example of mapping instruction mix blocks (Section III-A4) to MITE, DSB, and LSD. Each instruction mix block is 5 micro-ops (4 *mov* plus 1 *jmp*). If number of chained 5 micro-op blocks is 8 then all will fit in LSD (since  $8 \times 5 = 40 < 64$  micro-op limit of LSD) and they can all map to same DSB set (since DSB is 8-way associative).

vs. MITE+DSB timing differences to perform attacks related to DSB evictions through set collisions. On the other hand, the timing difference of processing using LSD vs. DSB will be used to perform attacks related to LSD evictions through misaligned accesses. Both of these also have power differences that separately can be used for power-based attacks.

### B. Generating DSB Evictions Through Set Collisions

To force frontend path changes, we set up a series of instruction mix blocks and align the start of the instruction address of each block to map to the same DSB set, as shown in Figure 5. We make the *jmp* instructions at the end of each instruction mix block jump to the first instruction of next instruction mix block. In this case, executing the first *mov* instruction of the first instruction mix block will trigger a series of instruction mix block execution. If the chain of instruction mix blocks is less than 12, all the blocks should fit in LSD. However, at the same time, each DSB set has 8 ways, so 8 blocks can map to same set. Consequently, if the chain of blocks is set to 8 (rather than 12), they can both fit in LSD and same DSB set. But, as soon as the chain is extended to 9 (or more) blocks that map to same set, eviction occurs in DSB, and in turn force LSD eviction due to inclusive nature of MITE, DSB, and LSD.

Inclusive feature of MITE, DSB, and LSD makes eviction of lines from DSB to cause flush of the LSD unit. Furthermore, eviction from DSB redirects micro-ops to be processed by MITE. Combining these, eviction from DSB will cause transition of micro-op delivery from LSD to both DSB and MITE.

Note that changing the chain of instruction mix blocks from 8 to 9 will not cause eviction or misses of L1 instruction cache. L1 instruction caches for the machines we tested are 8-way associative and contain 64 sets of 64 bytes. Consequently, the size of the L1 instruction is 4 times of DSB and instruction mix blocks mapping to the same DSB set will be mapped to different L1 instruction sets, as is shown in Figure 5. In other

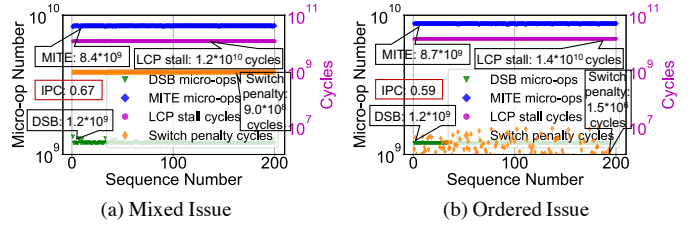


Fig. 6: Intel Xeon Gold 6226 CPU performance counter readings for the different experiments with ordered-issued or mixed-issued types of *add* instructions. The numbers in the call-out boxes are the average micro-ops numbers for all the 200 rounds of experiments.

words, changing chain length from 8 to 9 causes DSB and LSD eviction, but causes no misses in L1 instruction cache.

### C. Generating LSD Evictions Through Misaligned Accesses

We further found that misaligned instructions will generate collisions in the LSD, even when the number of total accessed instruction mix blocks does not exceed the DSB way number. This can be achieved by setting up the initial addresses of instruction mix blocks to be misaligned, e.g., by aligning them on 16 byte boundaries that are not multiple of 32 bytes.

The alignment or misalignment of the blocks will cause different frontend path changes when processing micro-ops. When all the instruction mix blocks are misaligned, executing 4 chained instruction mix blocks that map to the same DSB set will trigger collisions in LSD which causes the micro-op delivery change from LSD to DSB. At the same time, as we discussed in Section III-B, executing 4 chained instruction mix blocks that map to the same DSB set will use LSD unit since the size of the 4 blocks (of 5 micro-ops each) is less than 64 micro-op limit of the LSD.

When considering accessing pattern, if accessing a chain of 7 instruction mix blocks which are all aligned, the 8<sup>th</sup> access will determine the path used. If the 8<sup>th</sup> access is aligned, all of the micro-ops will still be processed by the LSD. While if the 8<sup>th</sup> instruction mix block is misaligned, LSD will be flushed and micro-ops will be redirected to use DSB in the frontend. We found that {aligned + misaligned} instruction mix block access pairs that will cause micro-ops to be changed from the LSD to the DSB paths are: {5 aligned + 2 misaligned}, {6 aligned + 2 misaligned}, {3 aligned + 3 misaligned}, {4 aligned + 3 misaligned}, and {5 aligned + 3 misaligned}. Similar to DSB evictions, misalignment will not cause L1 instruction cache misses.

### D. Generating Different DSB Switch Penalties

In x86, Length Changing Prefixes (LCPs) is designed and incorporated into the x86 ISA to identify the instructions with non-default length, which may appear with unicode processing and image processing [1]. For example, an instruction starting with *0x66h* prefix means there would be an operand size override, such prefix can force CPU to use slower decoding MITE path and incur up to 3 cycles more penalty in addition to extra DSB-to-MITE switch penalty.

To demonstrate that generating different switch penalties is feasible, we set up two instruction mix blocks. The first instruction mix block is filled by 16 sets of two *add* instructions, with one normal *add* instruction followed by one *add* instruction with length changing prefixes (mixed issue), and repeating this alternating pattern to the end. The second one is filled with 16 normal *add* instructions followed by 16 *add* instructions with length changing prefixes (ordered issue). In both cases there are 32 instructions within the loop and we iterate the loop for 800 million times. Figure 6 shows the results of the measurement. The two instruction blocks generate similar number of micro-ops from MITE and DSB, but with detectable difference in the final performance (IPC), which is caused by different numbers of LCP stall cycles and DSB-to-MITE switch penalty cycles. This shows that the same type of frequently-used instructions can come with different front-end path switching penalties.

We also found LCPs utilizable behaviors including a) it will force the front-end to switch from issuing instructions from DSB to issuing instructions from MITE, b) LCP instructions are only decoded sequentially and would incur measurable performance difference. Therefore, it is feasible to establish a covert channel base on instructions with LCP.

#### IV. PROCESSOR FRONTEND VULNERABILITIES

The vulnerabilities presented in this paper result in number of different new covert channels that can be used for attacks. In this section, we focus on timing-based channels and attacks. Power-based channels and attacks are discussed in Section VI. Meanwhile, application of the channels to attack SGX enclaves is presented in Section VII, and for use with Spectre attacks in Section VIII. Fingerprinting of the microcode patches, which can use both timing or power, is presented in Section IX.

Our attacks can be differentiated based on the techniques used to covertly send different bits by switching between different frontend paths: using eviction (following ideas in Section III-B), using misalignment (following ideas in Section III-C), or using LCP stalls and DSB-to-MITE switch penalties (following ideas in Section III-D).

For different attacks, there are three steps for all the attacks:

- **Init Step:** A series of instruction accesses are performed in this step to set the micro-ops into certain frontend paths, for some attacks no initial step is needed, only start timing (or power) measurements.
- **Encode Step:** The sender accesses certain instructions to change frontend paths of micro-ops previously set in the initialization step according to the secret bit to be sent.
- **Decode Step:** The receiver accesses certain instructions accessed, depending on attack type, timing (or power) is measured only for this step, or for all three steps.

Timing (or power) is measured just for the last step for multi-threading (MT) attacks (used for SGX attacks) and non-MT attacks (used for Spectre attacks), while there are also other types of timing (or power) where all steps are measured for non-MT attacks (used for SGX attacks).

In the attack description:  $N$  is the number of ways in the DSB,  $m$  is the a 1-bit message to transfer on the channel,  $d$  is

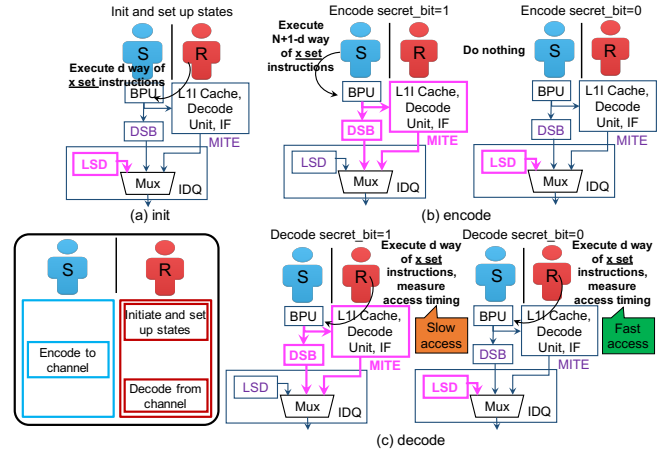


Fig. 7: Overview of the MT Eviction-Based Attack.

the different number of blocks used for each step,  $d < N + 1$ ,  $M$  (only used for misalignment-based attacks) is the parameters of the receiver,  $M < N + 1$ .  $p$  is the number of iterations the receiver requires for initialization and decoding step for one timing measurement.  $q$  is the number of iterations the sender requires for encoding step. Iteration is used to reliably observe timing result with low error rate.  $r$  (only used for attacks leveraging LCP) is the number of set of LCP instructions.

#### A. Eviction-Based Timing Attacks with Multi-Threading

For the eviction-based attacks, in a multi-thread (MT) setting, we deploy a sender thread and a receiver thread on a same physical processor core, but different hardware threads, which causes them to share the frontend. When the instruction stream from the sender executes, the DSB will be partitioned and the receiver's instructions will be evicted from DSB, further triggering eviction from LSD so that the delivery of instructions falls back from the LSD to DSB+MITE, therefore generating detectable timing signature that the receiver can measure. When the instruction stream from the sender is not executing, the receiver thread will use whole DSB and the evictions will not happen. This process leaves no interference in traditional instruction and data cache.

In this attack, the sender and the receiver use in total  $N + 1$  instruction mix blocks, denoted as lines 0 -  $N$ . For the MT eviction-based attack shown in Figure 7, in Init Step,  $d$  ( $d \leq N$ ) instruction mix blocks that map to a DSB set  $x$  are accessed for  $p$  times by the receiver. In Encode Step, the sender will execute different instruction series according to the secret bit  $m$ . When sending  $m = 1$ , the sender will execute  $N + 1 - d$  instruction mix blocks  $q$  times that map to DSB set  $x$ . In this case, the total ways accessed are larger than  $N$ , which causes eviction of DSB within the receiver and directs the micro-op delivery from LSD to DSB and MITE. When sending  $m = 0$ , the sender does nothing. In Decode Step, the receiver will access the same  $d$  blocks accessed in Init Step and time Decode Step's access  $p$  times. If eviction happened, receiver's micro-ops in Decode Step will be delivered from DSB and MITE, where longer timing is measured, indicating message  $m = 1$  was sent from the sender. On the other hand, if no

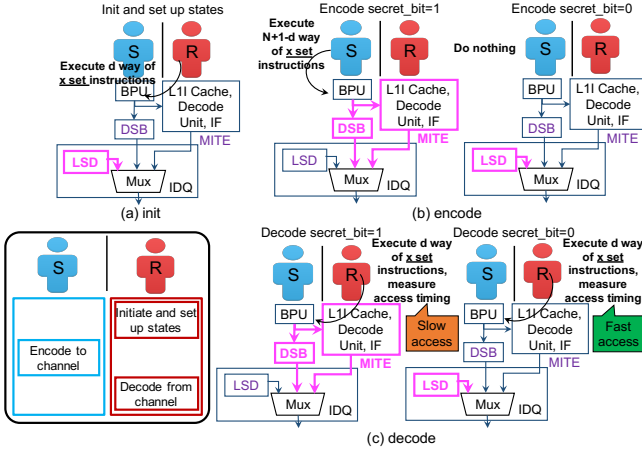


Fig. 8: Overview of MT Misalignment-Based Attack.

evictions happen, receiver’s micro-ops in Decode Step will still be delivered from LSD, where much shorter timing is observed compared to MITE+DSB path, indicating message  $m = 0$  is sent from the sender.

Take  $d = 6$  and  $N = 8$  for example (note that parameter  $M$  is not used for eviction-based attacks), the instruction access sequence when sending  $m = 1$  and  $m = 0$  are as follows:

- **Init:** access blocks 1 – 6 mapping to set  $x$
- **Encode:** access blocks 7 – 9 mapping to set  $x$  (if  $m = 1$ ); no access (if  $m = 0$ )
- **Decode:** access blocks 1 – 6 mapping to set  $x$  (if  $m = 1$ , DSB and MITE are used; if  $m = 0$ , LSD access is used)

### B. Misalignment-Based Timing Attacks with Multi-Threading

To achieve misaligned instruction access, sender and receiver first find virtual addresses of instructions that map to the same target set as what eviction-based attacks do, and then offset the initial address of every instruction mix blocks with 16 bytes (half of the DSB line size) to misalign the address.

For this type of attacks, the total number of instruction mix blocks of the sender and the receiver are equal to or less than  $N$  ways of the DSB, which has an advantage as it reduces the accesses and increases the transmission rate compared with eviction-based attacks.

The attack is shown in Figure 8. Here, the sender and the receiver use in total  $M$  ( $M \leq N$ ) instruction mix blocks. In Init Step and Decode Step, the receiver will access in total  $d$  (where  $d < N$ ) sets of instructions mix blocks that map to one DSB set for  $p$  times. In this case, the receiver’s instructions accessed in Init Step will be processed by the LSD. For the sender, in Encode Step, when sending  $m = 1$ , the sender will execute  $(M - d)$  (where  $M < N + 1$ ) sets of misaligned instructions that map to the same DSB set as the receiver for  $q$  times. In this case, misalignment of DSB causes the micro-op delivery to be redirected to DSB from LSD along with the aligned instruction access of the receiver, which leads to faster access of receiver’s instruction in Decode Step. When sending  $m = 0$ , the sender does nothing. In this case, all the micro-ops will still be delivered by the LSD and the receiver’s instruction access in Decode Step will derive slower access.

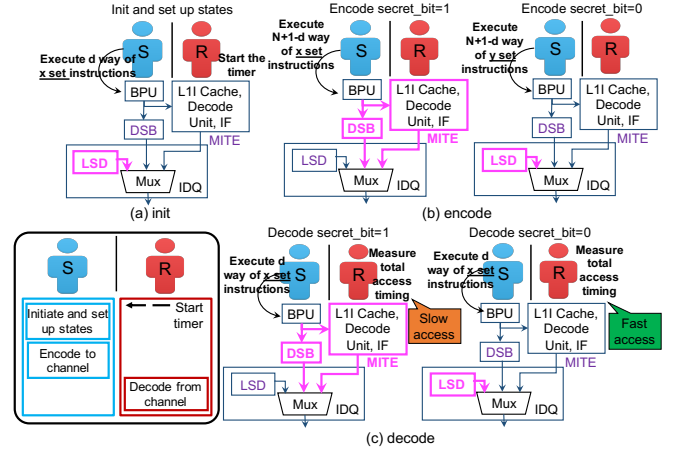


Fig. 9: Overview of Non-MT Stealthy Eviction-Based Attack.

Take  $d = 5, N = 8, M = 8$  for example, the access sequence when sending  $m = 1$  and  $m = 0$  are as follows:

- **Init:** access access blocks 1 – 5 mapping to set  $x$
- **Encode:** access *misaligned* blocks 6 – 8 mapping to set  $x$  (if  $m = 1$ ); no access (if  $m = 0$ )
- **Decode:** access blocks 1 – 5 mapping to set  $x$  (if  $m = 1$ , DSB access is used; if  $m = 0$ , LSD access is used)

### C. Eviction-Based Attacks without Multi-Threading

These attacks which do not leverage multi-threading, mainly require the sender to generate internal-interference or make the sender function interfere with the receiver function to transmit secret bit information. The receiver then measures the timing (or power, discussed later) to decode the information. Our attack using internal-interference of the sender is shown in Figure 9. The number of iterations of sender’s encoding ( $q$ ) and receiver’s initialization and decoding ( $p$ ) will be the same in this attack ( $p = q$ ) in order to reliably observe one timing result with low error rate. For one iteration, in Init Step, the receiver starts the timer in order to measure total time of the sender. The sender then executes  $d$  ( $d \leq N$ ) sets of instructions mix blocks that map to DSB set  $x$ . The instructions will be processed by the LSD. In Encode Step, When sending  $m = 1$ , the sender will execute  $N + 1 - d$  sets of instruction mix blocks that map to the same DSB set as the receiver. When sending  $m = 0$ , the sender will execute the same number of instructions but ones that map to a different DSB set  $y$  (stealthier for security) or do nothing (faster for bandwidth). In Decode Step, the sender will access the same  $d$  sets of instructions accessed in Init Step. Then the receiver will end the timer and calculate the total timing of the sender’s accesses to derive the information sent. If Encode Step’s access causes evictions, sender’s micro-ops in Decode Step will be delivered from DSB and MITE, where longer timing will be measured, indicating  $m = 1$  is sent from the sender. Otherwise,  $m = 0$  is transmitted from the sender.

Take  $d = 6$  and  $N = 8$  for example, the instruction access sequence when sending  $m = 1$  and  $m = 0$  are as follows:

- **Init:** access blocks 1 – 6 mapping to set  $x$

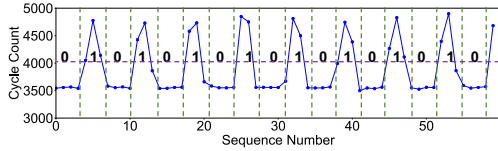


Fig. 10: Example trace of transmission of alternating 0s and 1s using the MT Eviction-Based channel, with  $d = 6$ , and threshold being set to 4000 cycle count (purple dotted line). Note this is not the fastest of the presented attacks in this paper.

- **Encode:** access blocks 7–9 mapping to set  $x$  (if  $m = 1$ ); 7–9 of set  $y$  (Stealthy) / no access (Fast) (if  $m = 0$ )
- **Decode:** access blocks 1–6 mapping to set  $x$  (if  $m = 1$ , DSB and MITE are used; if  $m = 0$ , LSD access is used)

#### D. Misalignment-Based Attacks without Multi-Threading

Similar to eviction-based non-MT attacks shown in Section IV-C, misalignment can also be used to generate interference without multi-threading. Details of this attack are not provided due to limited space.

Take  $d = 5, N = 8, M = 8$  for example, the instruction access sequence when sending  $m = 1$  and  $m = 0$  are as follows:

- **Init:** access blocks 1–5 mapping to set  $x$
- **Encode:** access *misaligned* blocks 6–8 mapping to set  $x$  (if  $m = 1$ ); *aligned* blocks 6–8 mapping to set  $x$  (Stealthy) / no access (Fast) (if  $m = 0$ )
- **Decode:** access block 1–5 mapping to set  $x$  (if  $m = 1$ , DSB access is used; if  $m = 0$ , LSD access is used)

#### E. Slow-Switch Attacks without Multi-Threading

Covert-channel attacks making use of LCP instructions are called slow-switch attacks. For slow-switch attacks, the attacker starts and ends the timer to measure sender’s interference in the Init and Decode Steps. In Encode Step, within the loop, there will be in total  $r$  number of LCP instructions being executed and the number of loops is  $p$  (or  $q$ ,  $p = q$  as the same setting for non-MT eviction-based attacks). When sending  $m = 1$ , the sender will alternatively execute one normal *add* instruction followed by one *add* instruction with length changing prefixes for  $r$  times. This instruction mix can enlarge the LCP stall cycles and maximize the DSB-to-LSD switches. When sending  $m = 0$ , the sender will execute  $r$  normal *add* instructions and then execute  $r$  *add* instruction with length changing prefixes. This instruction mix has less LCP stalls, at the same time minimizing the DSB-to-LSD switch penalties.

Take  $r = 16$  for example, the instruction access sequence when sending  $m = 1$  and  $m = 0$  are as follows:

- **Init:** start the timer.
- **Encode:** access 16 sets of *add* instruction with length changing prefixes and then normal *add* instructions (if  $m = 1$ ); access 16 normal *add* instruction and then 16 *add* instruction with length changing prefixes (if  $m = 0$ );
- **Decode:** stop the timer.

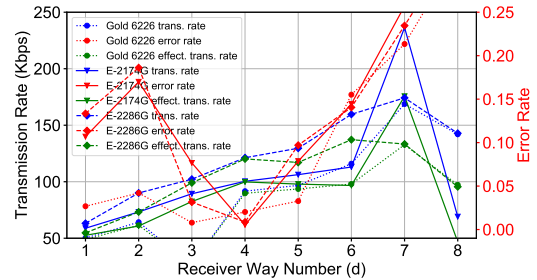


Fig. 11: Evaluation of MT Eviction-Based Attack for different values of parameter  $d$  (receiver way number).

## V. EVALUATION

In this section, we evaluate the bit transmission rates and error rates of all the timing attacks discussed in Section IV. Power attacks, SGX attacks, use of new covert channels in Spectre, and microcode patch fingerprinting are evaluated later.

The evaluation is conducted on 4 recent  $x86\_64$  processors from Intel Skylake’s family. The specifications of the processors is shown in Table I. For each covert channel, the transmitted data is compared with the received data to compute the error rates. To evaluate the error rates of the channel, the Wagner-Fischer algorithm [21] is used to calculate the edit distance between the sent string and the received string.

#### A. Number of Iterations ( $p, q$ ) for Attack Steps

After careful tuning of the configurations, when sending each bit  $m$  of message, non-MT attacks can have  $p = q = 10$  (to repeat initialize, encode, and decode steps and still reliably observe result with low error rates). To transmit each bit, the sender does one encoding step and receiver does one decoding step, hence  $p = q$ , and in total they are repeated 10 times. For MT attacks, for each bit to be transmitted, the receiver does 10 decoding measurements for each encoding step, and each encoding has to be repeated 100 times, hence  $p/q = 10$ , where  $q = 100$  (total encoding steps),  $p = 1000$  (total decoding steps). The  $q = 100$  is due to more noise in the MT setting, compared to  $q = 10$  for the non-MT setting.

#### B. Threshold for Detecting Transmitted Bit ( $m = 1$ vs. $m = 0$ )

Example trace of transmission of alternating 1s and 0s is shown in Figure 10. To establish decoding threshold for timing measurements, an alternating pattern of 0s and 1s is sent, and the timing (measured in cycles using the `rdtscp` instruction) is averaged for 0s and 1s to establish the threshold. Based on different covert channels, if a measurement is 30–70% or more above the threshold, it is judged to be a “1”, otherwise it is judged to be a “0”. The simple encoding can be in future replaced with other channel coding methods [20] for possibly faster transmission.

#### C. Influence of ( $d, M$ ) Parameters

To help find the ideal transmission rate, we evaluate the influence of  $d$  (number of ways accessed by the receiver)



TABLE II: Transmission rates and error rates of covert-channels when setting  $d = 1$  for MT Eviction-Based Attack for different message patterns: all 0s, all 1s, alternating 0s and 1s, and random.

	All 0s Message			All 1s Message			Alternating 0s and 1s Message			Random Message		
	G-6226	E-2174G	E-2286G	G-6226	E-2174G	E-2286G	G-6226	E-2174G	E-2286G	G-6226	E-2174G	E-2286G
<b>Tr. Rate (Kbps)</b>	42.66	49.53	87.33	55.28	61.17	102.39	50.21	58.86	64.96	18.28	21.80	25.61
<b>Error Rate</b>	0.00%	0.00%	0.00%	0.00%	0.00%	0.00%	2.68%	10.69%	12.56%	22.57%	18.53%	19.83%

TABLE III: Transmission rates and error rates of all the eviction-based and misalignment-based attacks when setting  $d = 6$  for eviction-based attacks and  $d = 5$ ,  $M = 8$  for misalignment-based attacks. The transmitted message is alternating 0s and 1s. Transmission rates for the fastest attack are shown in bold. Intel Xeon E-2288G machine we tested has hyper-threading disabled so there is no MT attacks.

	Non-MT Stealthy Eviction-Based				Non-MT Stealthy Misalignment-Based				MT Eviction-Based			
	G6226	2174G	2286G	2288G	G6226	2174G	2286G	2288G	G6226	2174G	2286G	2288G
<b>Tr. Rate (Kbps)</b>	419.67	851.81	1182.55	1356.43	713.01	466.02	723.15	1094.39	115.97	113.02	161.63	—
<b>Error Rate</b>	6.48%	3.43%	3.45%	0.36%	22.56%	11.34%	16.56%	10.08%	15.52%	14.44%	13.93%	—

	Non-MT Fast Eviction-Based				Non-MT Fast Misalignment-Based				MT Misalignment-Based			
	G6226	2174G	2286G	2288G	G6226	2174G	2286G	2288G	G6226	2174G	2286G	2288G
<b>Tr. Rate (Kbps)</b>	501.06	977.68	1205.90	1399.96	500.90	959.45	1228.35	<b>1410.84</b>	129.36	152.44	200.37	—
<b>Error Rate</b>	6.09%	0.00%	0.00%	0.00%	0.16%	0.00%	0.16%	<b>0.00%</b>	7.85%	2.77%	4.62%	—

TABLE IV: Transmission rates and error rates of Slow-Switch Attacks. The transmitted message is alternating 0s and 1s.

	Non-MT Slow-Switch-Based	
	G6226	2288G
<b>Tr. Rate (Kbps)</b>	678.11	1351.43
<b>Error Rate</b>	6.74%	0.64%

and its impact on the transmission rate and error rates.<sup>2</sup> The results of changing  $d$  for MT fast eviction-based Attack is shown in Figure 11. When increasing  $d$  from 1 to 8 (DSB has  $N = 8$  sets), the number of ways accessed by the sender will decrease (number of sender’s ways accessed is  $N + 1 - d$ ). Receiver’s observation will then become less stable (error rate increases) while on the other hand transmission rate increases. Error rates of small  $d$  (e.g.,  $d = 1, 2$ ) are also large because when the number of ways accessed by the receiver is small, timing difference of sending 0 and 1 is small which can be disrupted by the system noise. To find a balance between the transmission rate and error rate, we choose  $d = 6$  for eviction-based attacks. For misalignment-based attacks, we choose  $d = 5$ ,  $M = 8$  ( $M$  is the total number of ways accessed by the sender and receiver for misalignment-based attacks).

#### D. Influence of Message Patterns

A sample evaluation of MT eviction-based Attack for the four different message patterns with  $d = 1$  is shown in Table II. From the results it can be seen that better transmission rate and error rate are derived for all 0s and all 1s. This is mainly because when not changing the bits (as is case for all 0s or all 1s), the frontend path used by the sender accesses remains the same, generating less noise. The random messages are the worst due to the frequent frontend path changes.

#### E. Transmission Rates and Error Rates

The bit transmission rates and error rates for all types of the timing-based attacks are presented in Table III and Table IV,

with  $d = 6$  for eviction-based attacks,  $d = 5$  for misalignment-based attacks and  $r = 16$  for slow-switch attacks. For the best attack, which is the non-MT misalignment-based attack, the transmission rate can be as high as 1410 Kbps (1.41 Mbps) with almost 0% error rate.

In general, non-MT misalignment-based attacks have better transmission rate than the non-MT eviction-based attacks because non-MT misalignment-based attacks require fewer accesses (8 vs. 9) per loop iteration to transmit 1 bit of the message. Slow-switch attacks have generally similar transmission rate compared with the non-MT misalignment-based attacks. Non-MT attacks have better transmission rate than MT attacks due to smaller noise that allows for faster transmission.

## VI. POWER-CHANNEL ATTACKS

Switching between LSD or DSB and the MITE will not only cause timing changes for instruction processing, but also power changes. The power changes can be measured by abusing unprivileged access to Intel’s Running Average Power Limit (RAPL) interface [12].<sup>3</sup> Figure 12 shows example histogram of the power consumption of utilizing different frontend paths for the micro-ops in Intel Xeon Gold 6226 processor. Based on the power differences, we demonstrate a non-MT attack that can detect LSD or DSB vs. MITE frontend path power differences caused by eviction or misalignment through observing the power changes in RAPL. Configuration of the attack is similar to the non-MT attack demonstrated in Section IV-C. To observe the power differences, for each bit transmission the initialize, encode, and decode steps have to be iterated for  $p = q = 240,000$  times since RAPL interface update interval is around 20kHz [17]. The power attack’s bandwidth is limited by the update interval of RAPL, and is less than for the timing attacks.

Table V shows the evaluation results of two power-based non-MT attacks on Intel’s Xeon Gold 6226 processor. The bandwidth of the power attacks is around 0.6 – 0.7 Kbps. The transmission is still above 100 bps which is considered

<sup>2</sup>This work is not aimed at achieving the highest bandwidth covert channel. To fully optimize the transmission rate and error rate, techniques such as the ones used in [25] can be further exploited.

<sup>3</sup>In power attacks, if unprivileged RAPL accesses are prevented, we can still use privilege access and use power to attack SGX enclaves. We do not show this type of attack due to the limited space.

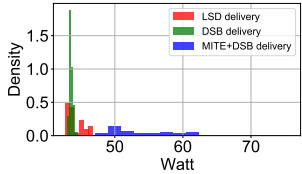


Fig. 12: Example histogram of power consumption when different frontend paths are used to process micro-ops in Intel Xeon Gold 6226 processor.

TABLE V: Power evaluation of Non-MT Power-Based attacks on Intel Xeon Gold 6226 processor when setting  $d = 6$ .

	Power Eviction-Based	Power Misalignment-Based
Tr. Rate (Kbps)	0.66	0.63
Error Rate	18.87%	9.07%

a high-bandwidth channel by TCSEC [22]. The power attack bandwidth can possibly be further improved using techniques such as the ones shown in recent PLATUPUS work [17].

## VII. ATTACKS ON SGX

The goal of Intel Software Guard Extension (SGX) is to protect sensitive data against the untrusted user, even on already compromised system, with the help of hardware-implemented security and cryptographic mechanism inside the processor [1]. Unfortunately, as we demonstrate, SGX is also vulnerable to frontend-related attacks.<sup>4</sup>

To demonstrate our attacks in an SGX environment, we assume a sender Trojan is running inside the SGX enclave and manipulates the use of the frontend paths to communicate to a receiver outside of the SGX. We consider both non-MT and MT SGX attacks, but for both there is only SGX entry and one SGX exit, while attacker measures the execution time from the outside. Consequently, instruction TLB flushing upon entry and exit does not impact our attacks.

1) *MT Timing-Based SGX Attacks*: For MT timing-based SGX attacks, the sender maintains its own thread and performs the covert transmission from within the enclave. Meanwhile, the receiver decodes bits of the sender by measuring the timing of its own operations. Under this scenario, because the frontend path components (MITE, DSB, and LSD) are shared between the enclave and non-enclave code, the receiver is able to detect the performance difference of its own instruction access based on the activity inside the SGX. If SGX thread is running, then the receiver will observe the partitioned DSB. If the SGX thread is idle, whole DSB is dedicated to the receiver thread. Receiver can observe its own internal-interference and deduce the DSB state.

Evaluation of the MT timing-based SGX attacks is shown in Table VI. It can be seen from the table that the transmission rates of SGX attacks can be roughly 6 Kbps – 15 Kbps with iteration numbers  $p = 1,000$ ,  $q = 10,000$ , while maintaining the similar error rates as the MT non-SGX attacks.

<sup>4</sup>We demonstrate attacks on SGX, although there is a newer SGX2 which extends SGX with dynamic memory management and other features, we believe these features will not affect our attacks and our attacks can be applied to SGX2 in future when machines with SGX2 are available.

2) *Non-MT Timing-Based SGX Attacks*: For non-MT timing-based SGX attacks, the sender Trojan is still inside the enclave, while the receiver derives the information by measuring the timing of SGX operation from outside of the enclave. Under this scenario, the receiver’s observations depend on ability to detect the internal interference of the sender’s accesses within the enclave, to detect whether there are frontend path changes caused by the eviction or misalignment of the micro-ops or not. The non-MT SGX attacks, because they do not leverage multi-threading, are possible even when multi-threading is disabled for security.

In the non-MT setup, we assume the attacker (receiver) is able to trigger the sender and they both execute on the same hardware thread. To reduce overhead and noise of enclave exits and entrances, for each transmission of a bit, there is only one entrance and exit. Effectively the receiver starts time measurement, then allows the enclave to run, and then finally measures the timing of the enclave as it was affected by the frontend paths. Compared to non-SGX attacks, more iterations of initialization, encoding, and decoding are necessary ( $p = q = 1,000 - 5,000$  iterations for the SGX attack compared to  $p = q = 10$  iterations for non-SGX attacks) in order to transmit one bit.

Evaluation of the non-MT timing-based SGX attacks is shown in Table VI. As the table shows, the transmission rates of non-MT SGX attacks are roughly 1/25 to 1/30 of non-MT non-SGX attacks, while still maintaining acceptable and even lower error rates.

3) *Power-Based SGX Attacks*: Power-based attacks are also possible, but not discussed due to limited space. We remark, however, that even if RAPL is disabled for user-level code, power-based SGX attacks are possible because RAPL can be accessed from the privileged, malicious OS.

## VIII. FRONTEND AND INSTRUCTION CACHE-BASED SPECTRE ATTACKS

Speculative attacks leverage transient execution to access secret and then a covert channel to pass the secret to the attacker [7], [16], [18]. In this section, we demonstrate our new variants of Spectre v1. In our Spectre attacks, we assume an in-domain attack where the victim and attacker code are in the same thread, so only one thread is running on the processor core. The secret message is represented by 5 bit chunks (each chunk can have value from 0 to 31). We then use one of the 32 DSB sets to represent each value. Similar to cache-based channels, during the speculative execution secret value is encoded by accessing the corresponding set. Unlike with cache attacks, to access a DSB set, instruction mix block mapping to that set has to be executed. We also implemented Spectre v1 attacks using L1I cache Flush + Reload attack and L1I Prime + Probe attack, to compare to our frontend attacks.

Table VII shows the L1 miss rate when using our channels compared to other channels. While our Spectre v1 attacks have lower bandwidths than data cache-based Spectre attacks, we are able to achieve lowest L1 miss rates. Especially, compared with recent cache-based LRU [35] covert channels which target stealthy attacks without causing high data cache miss

TABLE VI: Transmission rates and error rates of covert channels to attack SGX enclave when setting  $d = 6$  for eviction-based attacks and  $d = 5, M = 8$  for misalignment-based attacks. The transmitted message is alternating 0s and 1s. Intel Xeon E-2288G machine we tested has hyper-threading disabled so no MT attack data is provided for this machine.

SGX Attacks	Non-MT Stealthy Eviction-Based			Non-MT Stealthy Misalignment-Based			MT Eviction-Based		
	E-2174G	E-2286G	E-2288G	E-2174G	E-2286G	E-2288G	E-2174G	E-2286G	E-2288G
<b>Tr. Rate (Kbps)</b>	18.96	19.56	21.20	23.93	24.70	27.10	7.85	14.89	—
<b>Error Rate</b>	0.16%	1.33%	2.18%	0.32%	0.76%	0.76%	6.74%	8.02%	—
SGX Attacks	Non-MT Fast Eviction-Based			Non-MT Fast Misalignment-Based			MT Misalignment-Based		
	E-2174G	E-2286G	E-2288G	E-2174G	E-2286G	E-2288G	E-2174G	E-2286G	E-2288G
<b>Tr. Rate (Kbps)</b>	29.35	32.01	34.48	30.36	31.18	35.20	6.39	13.62	—
<b>Error Rate</b>	0.04%	1.40%	0.40%	0.08%	1.08%	0.68%	2.56%	12.95%	—

TABLE VII: L1 miss rates of our Spectre v1 version attack (run on Intel’s Xeon Gold 6226 processor) with variants of Spectre v1 that use different covert channels. MEM F+R, L1D F+R, and L1D LRU attacks are from work [35]. L1 miss rates in [35] are L1D miss rates.

	Others			Our		
	MEM F+R [35]	L1D F+R [35]	L1D LRU [35]	L1I F+R	L1I P+P	Frontend
<b>L1 Miss Rate</b>	2.81%	4.79%	4.48%	0.45%	0.48%	0.21%

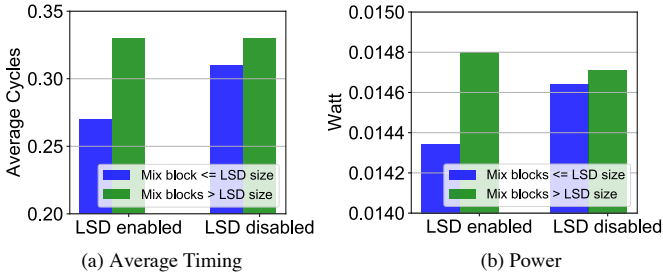


Fig. 13: Example comparison of frontend timing and power for executing instruction mix blocks less or greater than LSD capacity. All mix blocks map to the same DSB set. If LSD is disabled execution falls back to DSB and MITE.

rates, our frontend attack does not cause any cache misses at all, making the L1 miss rate the smallest.

## IX. MICROCODE PATCH DETECTION

When evaluating the behavior of the processor frontend, we also found a new type of attack where performance of the frontend can be used for fingerprinting the microcode updates of the processor. In particular, we evaluated our Intel Xeon Gold 6226 test machine under older 3.20180312.0ubuntu18.04.1 (patch1) and newer 3.20210608.0ubuntu0.18.04.1 (patch2) Intel microcode patches. While neither patch explicitly mentions LSD, we found that with the newer patch2 LSD is disabled while with older patch1 the LSD is enabled. To switch between the patches, the processor has to be restarted so the microcode in the CPU can be updated.

To detect the changes in the LSD behavior, we can use both the timing difference and the power difference when testing code sequences with number of instruction mix blocks less than LSD capacity (so they would fit in LSD and be processed by LSD) or sequences with number of instruction mix blocks greater than LSD capacity (so micro-ops would be forced to be handled by DSB and MITE instead). The average timing and power difference for LSD enabled (patch1)

vs. disabled (patch2) are shown in Figure 13. Attackers can clearly differentiate which patch has been applied, with timing being a more reliable indicator.

Attackers can leverage this to learn of vulnerabilities of the processor. For example, patch2<sup>5</sup> protects against CVE-2021-24489: potential security vulnerability in some Intel Virtualization Technology for Directed I/O (VT-d) products that allows for escalation of privilege. Knowing the patch is applied or not allows the attacker to exploit VT-d related attacks. The frontend timing thus can not only be the target of attack itself, but help attacker discover other vulnerabilities in the system.

## X. CONCLUSION

This paper evaluated security vulnerabilities in processor frontends. The work demonstrated numerous threats due to DSB and LSD. Further it showed SGX attacks, version of Spectre attack, and a new microcode fingerprinting approach. This work demonstrated that the whole processor frontend needs to be considered to ensure processor security, especially as the presented attacks and covert transmission bandwidths can surpass 1Mbps in many cases.

## ACKNOWLEDGEMENT

Shuwen Deng was supported by a Google PhD Fellowship. This work was also supported in part NSF grant 1813797 and through SRC award number 2844.001. We thank Abhishek Bhattacharjee for his insightful comments and feedback.

## REFERENCES

- [1] “Intel 64 and ia-32 architectures software developer’s manual: Volume 3,” <https://www.intel.com/content/www/us/en/architecture-and-technology/64-ia-32-architectures-software-developer-system-programming-manual-325384.html>.
- [2] “Snoop-assisted l1 data sampling,” <https://software.intel.com/security-software-guidance/advisory-guidance/snoop-assisted-l1-data-sampling>.
- [3] A. C. Aldaya, B. B. Brumley, S. ul Hassan, C. P. Garcia, and N. Tuveri, “Port contention for fun and profit,” in *2019 IEEE Symposium on Security and Privacy (SP)*. IEEE, 2019, pp. 870–887.
- [4] D. J. Bernstein, “Cache-timing attacks on aes,” 2005.
- [5] A. Bhattacharyya, A. Sandulescu, M. Neugschwandner, A. Sorniotti, B. Falsafi, M. Payer, and A. Kurmus, “Smotherspectre: exploiting speculative execution through port contention,” in *Conference on Computer and Communications Security*, 2019, pp. 785–800.
- [6] C. Canella, D. Genkin, L. Giner, D. Gruss, M. Lipp, M. Minkin, D. Moghimi, F. Piessens, M. Schwarz, B. Sunar *et al.*, “Fallout: Leaking data on meltdown-resistant cpus,” in *Proceedings of the 2019 ACM SIGSAC Conference on Computer and Communications Security*, 2019, pp. 769–784.

<sup>5</sup>Patch2 adds protections against CVE-2021-24489, CVE-2020-24511, CVE-2020-24512, and CVE-2020-24513.

- [7] C. Canella, J. Van Bulck, M. Schwarz, M. Lipp, B. Von Berg, P. Ortner, F. Piessens, D. Evtvushkin, and D. Gruss, "A systematic evaluation of transient execution attacks and defenses," in *28th {USENIX} Security Symposium ({USENIX} Security 19)*, 2019, pp. 249–266.
- [8] A. C. De Melo, "The new linux perf tools," in *Slides from Linux Kongress*, vol. 18, 2010, pp. 1–42.
- [9] S. Deng and J. Szefer, "New predictor-based attacks in processors," in *Proceedings of the Design Automation Conference*, ser. DAC, December 2021.
- [10] D. Evtvushkin, D. Ponomarev, and N. Abu-Ghazaleh, "Jump over aslr: Attacking branch predictors to bypass aslr," in *2016 49th Annual IEEE/ACM International Symposium on Microarchitecture (MICRO)*. IEEE, 2016, pp. 1–13.
- [11] D. Evtvushkin, R. Riley, N. C. Abu-Ghazaleh, ECE, and D. Ponomarev, "Branchscope: A new side-channel attack on directional branch predictor," *ACM SIGPLAN Notices*, vol. 53, no. 2, pp. 693–707, 2018.
- [12] C. Gough, I. Steiner, and W. Saunders, *Energy efficient servers: blueprints for data center optimization*. Springer Nature, 2015.
- [13] B. Gras, K. Razavi, H. Bos, and C. Giuffrida, "Translation leak-aside buffer: Defeating cache side-channel protections with {TLB} attacks," in *27th {USENIX} Security Symposium ({USENIX} Security 18)*, 2018, pp. 955–972.
- [14] D. Gruss, C. Maurice, A. Fogh, M. Lipp, and S. Mangard, "Prefetch side-channel attacks: Bypassing smap and kernel aslr," in *Proceedings of the 2016 ACM SIGSAC conference on computer and communications security*, 2016, pp. 368–379.
- [15] D. Gruss, C. Maurice, K. Wagner, and S. Mangard, "Flush+ flush: a fast and stealthy cache attack," in *International Conference on Detection of Intrusions and Malware, and Vulnerability Assessment*. Springer, 2016, pp. 279–299.
- [16] P. Kocher, J. Horn, A. Fogh, D. Genkin, D. Gruss, W. Haas, M. Hamburg, M. Lipp, S. Mangard, T. Prescher *et al.*, "Spectre attacks: Exploiting Speculative Execution," in *Symposium on Security and Privacy (S&P)*, 2019, pp. 1–19.
- [17] M. Lipp, A. Kogler, D. Oswald, M. Schwarz, C. Easdon, C. Canella, and D. Gruss, "Platypus: Software-based power side-channel attacks on x86," in *IEEE Symposium on Security and Privacy (SP)*, 2021.
- [18] M. Lipp, M. Schwarz, D. Gruss, T. Prescher, W. Haas, A. Fogh, J. Horn, S. Mangard, P. Kocher, D. Genkin *et al.*, "Meltdown: Reading kernel memory from user space," in *27th {USENIX} Security Symposium ({USENIX} Security 18)*, 2018, pp. 973–990.
- [19] F. Liu, Y. Yarom, Q. Ge, G. Heiser, and R. B. Lee, "Last-level cache side-channel attacks are practical," in *2015 IEEE symposium on security and privacy*. IEEE, 2015, pp. 605–622.
- [20] J. L. Massey, "Foundation and methods of channel encoding," in *Proc. Int. Conf. Information Theory and Systems*, vol. 65. NTG-Fachberichte, 1978, pp. 148–157.
- [21] G. Navarro, "A guided tour to approximate string matching," *ACM computing surveys (CSUR)*, vol. 33, no. 1, pp. 31–88, 2001.
- [22] "DoD 5200.28-STD, Department of Defense Trusted Computer System Evaluation Criteria," 1983, <http://csrc.nist.gov/publications/history/dod85.pdf>.
- [23] R. Paccagnella, L. Luo, and C. W. Fletcher, "Lord of the ring (s): Side channel attacks on the cpu on-chip ring interconnect are practical," *arXiv preprint arXiv:2103.03443*, 2021.
- [24] X. Ren, L. Moody, M. Taram, M. Jordan, D. M. Tullsen, and A. Venkat, "I see dead  $\mu$ ops: Leaking secrets via intel/amd micro-op caches," in *2021 ACM/IEEE 48th Annual International Symposium on Computer Architecture (ISCA)*. IEEE, 2021.
- [25] G. Saileshwar, C. W. Fletcher, and M. Qureshi, "Streamline: A fast, flushless cache covert-channel attack by enabling asynchronous collusion," 2021.
- [26] M. Schwarz, M. Lipp, D. Moghimi, J. Van Bulck, J. Stecklina, T. Prescher, and D. Gruss, "Zombieload: Cross-privilege-boundary data sampling," in *Proceedings of the 2019 ACM SIGSAC Conference on Computer and Communications Security*, 2019, pp. 753–768.
- [27] M. Schwarz, M. Schwarzl, M. Lipp, J. Masters, and D. Gruss, "Net-spectre: Read arbitrary memory over network," in *European Symposium on Research in Computer Security*. Springer, 2019, pp. 279–299.
- [28] D. Skarlatos, M. Yan, B. Gopireddy, R. Sprabery, J. Torrellas, and C. W. Fletcher, "Microscope: enabling microarchitectural replay attacks," in *2019 ACM/IEEE 46th Annual International Symposium on Computer Architecture (ISCA)*. IEEE, 2019, pp. 318–331.
- [29] C. Trippel, D. Lustig, and M. Martonosi, "Meltdownprime and Spectreprime: Automatically-Synthesized Attacks Exploiting Invalidation-Based Coherence Protocols," *arXiv preprint arXiv:1802.03802*, 2018.
- [30] J. Van Bulck, M. Minkin, O. Weisse, D. Genkin, B. Kasikci, F. Piessens, M. Silberstein, T. F. Wenisch, Y. Yarom, and R. Strackx, "Foreshadow: Extracting the keys to the intel {SGX} kingdom with transient out-of-order execution," in *27th {USENIX} Security Symposium ({USENIX} Security 18)*, 2018, pp. 991–1008.
- [31] J. Van Bulck, D. Moghimi, M. Schwarz, M. Lipp, M. Minkin, D. Genkin, Y. Yuval, B. Sunar, D. Gruss, and F. Piessens, "LVI: Hijacking Transient Execution through Microarchitectural Load Value Injection," in *41th IEEE Symposium on Security and Privacy (S&P'20)*, 2020.
- [32] S. van Schaik, A. Milburn, S. Österlund, P. Frigo, G. Maisuradze, K. Razavi, H. Bos, and C. Giuffrida, "RIDL: Rogue in-flight data load," in *S&P*, May 2019.
- [33] Y. Wang, A. Ferraiuolo, and G. E. Suh, "Timing channel protection for a shared memory controller," in *2014 IEEE 20th International Symposium on High Performance Computer Architecture (HPCA)*. IEEE, 2014, pp. 225–236.
- [34] O. Weisse, J. Van Bulck, M. Minkin, D. Genkin, B. Kasikci, F. Piessens, M. Silberstein, R. Strackx, T. F. Wenisch, and Y. Yarom, "Foreshadowing: Breaking the virtual memory abstraction with transient out-of-order execution," 2018.
- [35] W. Xiong and J. Szefer, "Leaking information through cache lru states," in *2020 IEEE International Symposium on High Performance Computer Architecture (HPCA)*. IEEE, 2020, pp. 139–152.
- [36] Y. Yarom and K. Falkner, "Flush+ reload: A high resolution, low noise, 13 cache side-channel attack," in *23rd {USENIX} Security Symposium ({USENIX} Security 14)*, 2014, pp. 719–732.